DEVELOPMENT OF SUPERCONDUCTING MATERIALS FOR USE IN MAGNET APPLICATIONS: Nb3Sn FLUX PINNING AND Bi-2212 MAGNETIC TEXTURING

A Senior Scholars Thesis

by

DAVID GABRIEL RAHMANI

Submitted to the Office of Undergraduate Research
Texas A&M University
in partial fulfillment of the requirements for the designation as

UNDERGRADUATE RESEARCH SCHOLAR

April 2010

Major: Physics

DEVELOPMENT OF SUPERCONDUCTING MATERIALS FOR USE IN MAGNET APPLICATIONS: Nb3Sn FLUX PINNING AND Bi-2212 MAGNETIC TEXTURING

A Senior Scholars Thesis

by

DAVID GABRIEL RAHMANI

Submitted to the Office of Undergraduate Research
Texas A&M University
in partial fulfillment of the requirements for the designation as

UNDERGRADUATE RESEARCH SCHOLAR

Approved by:

Research Advisor: Peter McIntyre
Associate Dean for Undergraduate Research: Robert C. Webb

April 2010

Major: Physics

ABSTRACT

Development of Superconducting Materials for Use in Magnet Applications: Nb3Sn Flux Pinning and Bi-2212 Magnetic Texturing. (April 2010)

David Gabriel Rahmani
Department of Physics and Astronomy
Texas A&M University

Research Advisor: Dr. Peter McIntyre
Department of Physics and Astronomy

The objective of this study was to develop techniques to be used in the manufacture of superconducting round wires for use in magnet applications. Nb_3Sn and Bi-2212 are superconducting materials currently being developed for the next generation of magnet technology. Flux pinning in Nb_3Sn has yet to be optimized, and the current carrying capacity of Bi-2212 is significantly lower than what is needed for practical use in high field magnets. Processes developed for the manufacture of Nb_3Sn and Bi-2212 as round wires are presented and discussed.

Processes were developed to increase flux pinning in Nb_3Sn by utilizing powder metallurgy techniques to introduce a heterogeneously homogenous distribution of nanoscale inclusions of candidate materials in Nb rod. The Nb rod is to be used in the fabrication of high-performance Nb_3Sn superconducting wire via a Powder-in-Tube method, in which the inclusions would act as artificial pinning centers. Consolidation of the powders via cold isostatic pressing proved problematic due to the high oxygen

content of commercially available Nb powder. Severe plastic deformation of Nb was investigated as a method to produce low oxygen content Nb powder. The prospect of using an inductively coupled plasma torch to remove the oxygen from commercially available Nb powder is also discussed.

An attempt was made to increase the current carrying capabilities of Bi-2212 by developing a procedure for magnetically texturing Bi-2212 powder with the goal of producing an Ag/Bi-2212 multifilamentary round wire with superior properties in high magnetic fields. In currently produced Bi-2212 wires, the conducting planes of each crystal are poorly aligned, and as a result, current transport is diminished. This project involves suspending Bi-2212 in a liquid solution on a substrate in the presence of a magnetic field in order to texture the deposited powder. This is possible because of the anisotropic magnetic susceptibility of Bi-2212. The solvent is then evaporated, leaving only the Bi-2212 powder on the substrate. The development of this process entailed optimizing the deposition method and observing the magnetic orientation of the powder.

ACKNOWLEDGMENTS

I would like to thank my advisor, Dr. Peter McIntyre, without whom this project would not have been possible. I would also like to thank Kyle Damborsky, Nathaniel Pogue, and Feng Lu for their gracious help in the lab. Thanks to Dr. Joseph Ross of the Department of Physics and Astronomy for allowing the use of his research group's magnet. Thanks as well to Andrew Jaisle and Nick Diaczencko for their assistance in the machining of Nb powder. Additional thanks to Raymond Blackburn and Tim Elliott for their help with the project. Thanks to Dr. Al McInturf and Dr. Akhdiyor Sattarov for their insight. Thanks also to Dr. Suveen Mathaudhu, at the US Army Research Lab, for his assistance. Finally, I would like to thank my friends and family for their support in all that I do.

NOMENCLATURE

APC	Artificial Pinning Centers
B	Magnetic Field
Bi-2212	Bismuth Strontium Calcium Copper Oxide
CIP	Cold Isostatic Pressing
EDS	Energy Dispersive Spectroscopy
EtOH	Ethanol
H_c	Critical Magnetic Field
HIP	Hot Isostatic Pressing
ICP	Inductively Coupled Plasma
J_c	Critical Current Density
MeOH	Methanol
MJR	Modified Jellyroll
PIT	Powder-in-Tube
ppm	Parts Per Million
RGA	Residual Gas Analysis
SEM	Scanning Electron Microscopy
SPD	Severe Plastic Deformation
T	Tesla
XRD	X-Ray Diffraction

TABLE OF CONTENTS

CHAPTER Page

LIST OF FIGURES

FIGURE Page

LIST OF TABLES

CHAPTER I

INTRODUCTION

The objective of this study was to develop superconductor technology, specifically with regards to round wires for use in magnet applications. Two different materials were used in this study: Nb_3Sn and $Bi_2Sr_2CaCu_2O_8$ (Bi-2212). While unrelated, both superconductors are potential materials for use in the next generation of high field magnets. Currently, Nb_3Sn is widely used in magnet applications; however, its flux pinning has not yet been optimized [1]. Bi-2212 is a newer material that is significantly more expensive and less widely used than Nb_3Sn or NbTi; however, it's critical current density (J_c) in single crystal samples has shown that it is capable of producing magnets of at least 45 T. Round wires of Bi-2212 are currently manufactured, but the preferred method has not been perfected. With enhanced flux pinning, Nb_3Sn can be used to make better performing high field magnets than are currently in use. Similarly, the successful development of Bi-2212 would enable the material to be used more widely and at a lower cost.

The structure of this thesis is covered here. Chapter II fully introduces the Nb_3Sn project. Chapter III covers the materials and methods used in the development of Nb_3Sn. Chapter IV discusses the data and results, including the microscopy and analysis

---

This thesis follows the style of *IEEE Transactions on Applied Superconductivity*.

of the samples. Chapter V summarizes the problems encountered with our approach. In Chapter VI, the methods of obtaining low oxygen content Nb powder are discussed. The Nb_3Sn project is concluded in Chapter VII. In Chapter VIII, the Bi-2212 project is introduced. Chapter IX covers the method of wire production for Bi-2212. The materials and methods used in the Bi-2212 project are discussed in Chapter X. Chapter XI contains the results, and the Bi-2212 project is concluded in Chapter XII. Chapter XIII is an overall conclusion of the general project.

CHAPTER II

INTRODUCTION TO Nb3Sn PROJECT

The objective of this research project is to devise a method to successfully implement flux pinning centers in niobium rod, for use in Nb_3Sn superconducting wire. Nb_3Sn superconductor is widely used to build superconducting magnets for Nuclear Magnetic Resonance, for use in mass spectrometers, and for confinement magnets in Nuclear Fusion reactors. Nb_3Sn is also a candidate material for use in future particle accelerator magnets. Most notably, it features a high current carrying capacity in the presence of background magnetic fields (B) that are significantly greater than the operational range of the traditional magnet winding material, NbTi. Furthermore, Nb_3Sn wire maintains these properties when manufactured in round wire form, making it more applicable for producing highly homogenous magnetic fields than the high temperature superconductors YBCO (tape only) and Bi-2212 (low critical current density) that have superior properties. Both Bi-2212 and YBCO have greater upper critical magnetic fields (H_c), and YBCO has a better current density as well [2]. The current carrying capabilities, quantitatively described as J_c vs. B of both Nb_3Sn and NbTi are shown in Figure 1 [1] along with their normalized pinning force curves. As the background magnetic field increases, the amount of force required to keep an individual flux vortex at a pinning site also increases. The maximum point in the normalized pinning curve represents the optimum magnetic field for pinning. NbTi is considered an optimized conductor, whereas the Nb_3Sn pinning curve is shifted to the low field region, indicating

the possibility of better J_c vs. B characteristics for Nb_3Sn if pinning is improved. Thus, the successful implementation of flux pinning centers in a manner that is conducive to large-scale industrial production has benefits that would affect the entire superconductor industry.

Flux pinning has been shown to occur at grain boundaries and at non-superconducting or poorly superconducting inclusions in a superconducting material [3]-[6]. Currently, flux pinning in Nb_3Sn is obtained by forming very fine grain boundaries. This type of flux pinning has increased the J_c at medium level magnetic fields of approximately 5 Tesla (T); however, the magnetic field at which the peak in J_c occurs has not shifted considerably by reducing the grain size [6]. The pinning force for Nb_3Sn and NbTi are shown in the inset of Figure 1 [1]. As can be seen, the maximum pinning force in Nb_3Sn occurs at approximately 20% of the critical magnetic field. However, it has been shown that by the use of artificial pinning centers, the peak in flux pinning force can be shifted to higher magnetic fields [5]. Previous experiments have demonstrated that the placement of artificial pinning centers (APCs) in thin films of Nb_3Sn increased the J_c in fields up to 12 T [7]. Additional experiments have shown that the highest J_c occurred in Nb_3Sn with Y and Ti acting as the APCs [8].

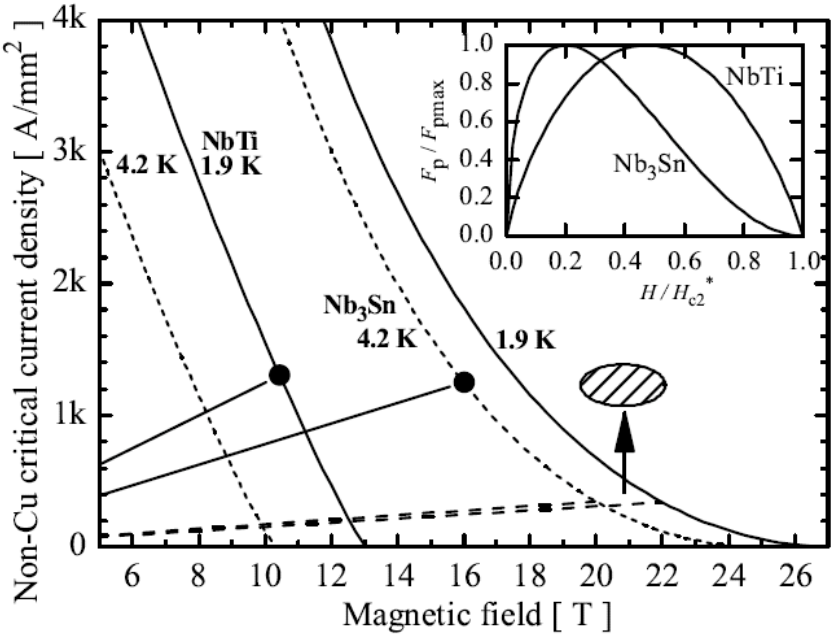

Fig. 1. J_c vs. B for NbTi and Nb_3Sn. Inset shows the normalized pinning force as a function of reduced magnetic field.

In recent years, APCs have been placed in Nb_3Sn wire by placing a Nb rod in a Cu tube which was then extruded to different diameters [9]. The extruded filaments were then bundled, extruded, and bundled with Sn filaments to form multifilamentary wires. The end result was Nb_3Sn wire with Cu strands dispersed through the length of the wire. In this study, the Cu strands acted as the APCs. This method of placing APCs in Nb_3Sn wire was shown to have shifted the peak of the pinning force to the right. However, the copper area fraction of these conductors was very large, and the critical current densities were not shown to improve via this method. In this study, the artificial pinning centers were long but fine Cu strands, as opposed to our method, which includes a homogenous distribution of nanometer sized particles, with the potential for long but fine ribbons of pinning centers.

In this thesis, we attempt to place nanometer sized APCs homogenously throughout the Nb_3Sn wire. This is done by using powder metallurgy techniques to disperse candidate materials throughout the bulk of Nb rod, which will be formed into a tube to be used in the Powder-in-Tube (PIT) method to form Nb_3Sn round wire. After our initial attempt at consolidating the powders, we discovered that the oxygen content in the Nb powder that we used was 3000 parts per million (ppm), which is prohibitively high. The high oxygen content decreases the malleability and ductility of the powder. This decreases the effectiveness of the powder metallurgy processes that we employ, as well as make the extrusion of wire more difficult. In addition, the higher oxygen content is detrimental to the superconductivity of the material. Based on previous work, our goal for oxygen content in Nb powder is 200 ppm [4]. Unfortunately, all currently commercially available Nb powder has oxygen contents that are greater than 2000 ppm, which are too high for our purposes. Because of this, we must manufacture low oxygen content Nb powder in order to use it for the placement of APCs.

We look at two methods of powder production. The first method entails manufacturing the powder by Severe Plastic Deformation (SPD), specifically, through a chip forming process. This process entails machining bulk Nb with various tools, rake angles, and speeds to produce chips of various sizes [10]. Chip sizes in the range of 100-200 micrometers are obtainable, which we believe to be sufficient for our purposes. Starting with bulk Nb, we can machine off the outer layer of the material, which is typically

oxidized, to be left with pure Nb bulk. Using low cutting speeds, heating of the Nb can be prevented. Performing the machining in an inert atmosphere, we can prevent the oxidation of the remaining Nb during machining, ending with low oxygen content Nb powder. This is a relatively low cost method compared to the plasma torch method; however, manufacturing industrial sized amounts of Nb powder is not likely.

The other method we investigate is the use of a plasma torch to remove the oxygen from commercially available Nb powder. This method utilizes a plasma torch to heat the powder past its melting point in an inert environment, removing the oxygen from the powder. The process is commercially available, and can reduce the oxygen content by a factor of ten with each pass through the plasma torch. Starting with powder containing 3000 ppm, an oxygen content of less than 100 ppm can be achieved with two passes. The benefit of this process is the ease of increasing to an industrial scale; however it does entail a high cost at the research level.

CHAPTER III

MATERIALS AND METHODS OF Nb3Sn PROJECT

Niobium rods with potential APCs for use in a Nb_3Sn superconducting, multifilament round wire were created through a CIP process as a precursor to a consolidating HIP process. To control mechanical and flux pinning properties, Y, Y_2O_3, Zr, W, Ti, and Cu metal powders were blended in measured quantities with Nb powder, then run through a CIP cycle, which peaked at 50,000 psi, with the intent of achieving a partially dense rod of approximately 80% density.

High purity powders, with sizes and purities shown in Table 1, were used in this experiment. Note that the Nb purity refers only to metallic impurities, and the Nb powder had a manufacturer's specification of 3000 ppm oxygen. All of the powders were shipped to Dr. Suveen Mathaudhu at the U.S. Army Research Laboratory (USARL) in Maryland for mixing. The yttrium powder was previously stored in an argon filled glove-box at the Magnet Lab at Texas A&M and was sealed in an argon filled container before shipment. The remaining powders were shipped in their original packaging.

TABLE I
Powder Sizes and Purities

Material	Purity	Particle Size	Company
Nb*	99.80%	1-5 micrometer	AEE
Y	99.90%	425 micrometer max	ESPI
Y_2O_3	99.95%	30-50 nm avg. part. size	Inframat
Ti	99.80%	45 micrometer max	AEE
Cu	Unknown	Unknown	USARL
W	Unknown	Unknown/nanoscale	Dr. Hartwig
Zr	99.70%	20 micrometer typical	Cerac

Upon receipt at USARL, the Y_2O_3 powder was heated at 80 °C for 1 h to reduce agglomeration. Powders were then mixed in twelve batches with masses given by Table 2 and atomic percentage by Table 3. After mixing, the powders were sent to Bodycote IMT Inc. in Andover, Massachusetts for the CIP cycle. Each sample was transported in a high density polyethylene bottle. Powders were transported sealed in argon filled containers. All handling of powders at Bodycote was carried out in an argon filled glove-bag. Once received by Bodycote, the samples were mixed by high energy blending to ensure a homogenous distribution of particles. The high energy blending occurred in the high density polyethylene bottles they were transported in.

TABLE II
Mass Composition (g)

Sample #	Nb	Y_2O_3	W	Zr	Ti	Y	Cu
1	771.3						
2	749.29					14.63	
3	707.6	35.83				14.11	
4	738.1		30.43			14.72	
5	715.55			14.95	7.85	14.57	
6	676.19					30.14	6.27
7	745.04				7.92	7.35	
8	734.09				7.88	14.64	
9	727.53					29.01	
10	674.15	69.73			7.39		
11	709.16			14.82		28.88	
12	663.6			15.52	8.15	15.12	6.27

TABLE III
Atomic Percentage (%)

Sample #	Nb	Y_2O_3	W	Zr	Ti	Y	Cu
1	100	0	0	0	0	0	0
2	98	0	0	0	0	2	0
3	96	2	0	0	0	2	0
4	96	0	2	0	0	2	0
5	94	0	0	2	2	2	0
6	94.25	0	0	0	0	4.5	1.25
7	97	0	0	0	2	1	0
8	96	0	0	0	2	2	0
9	96	0	0	0	0	4	0
10	94	4	0	0	2	0	0
11	94	0	0	2	0	4	0
12	92	0	0	2.25	2.25	2.25	1.25

The CIP cycle begins by loading the powders into a latex sleeve to a height of 4”. Some samples lacked sufficient powder to reach the 4” height, so steel risers of approximately ¼” thickness were inserted beneath the CIP bag to elevate the powder level. The sleeve is then placed inside a cylindrical steel can to form the desired rod geometry. A second latex sleeve is placed over the top of the powder and the two latex sleeves are sealed with electrical tape. The tube in the top sleeve is used to pull a vacuum on the powder. To prevent the powder from escaping the CIP bag, a cotton filter is placed between the evacuation tube and the latex surface. A sample bag loaded with powder can be seen in Figure 2.

Fig. 2. Sample with crimped hose after evacuation.

After the CIP bag is evacuated and crimped, a batch of six samples is loaded onto the stainless steel CIP rack. The CIP cans are zip tied in pairs to the rack, spaced every 120° around the circular rack. The CIP rack is then lowered into the CIP chamber which is filled with water and an anti-rust solution. After sealing the chamber, more fluid is pumped in through the bottom of the chamber until the pressure read at the fluid input exceeds 50,000 psi. At this point the pressure is maintained for approximately 1 minute, after which the pressure is slowly decreased. Each batch followed the same pressure cycle which is shown in Figure 3.

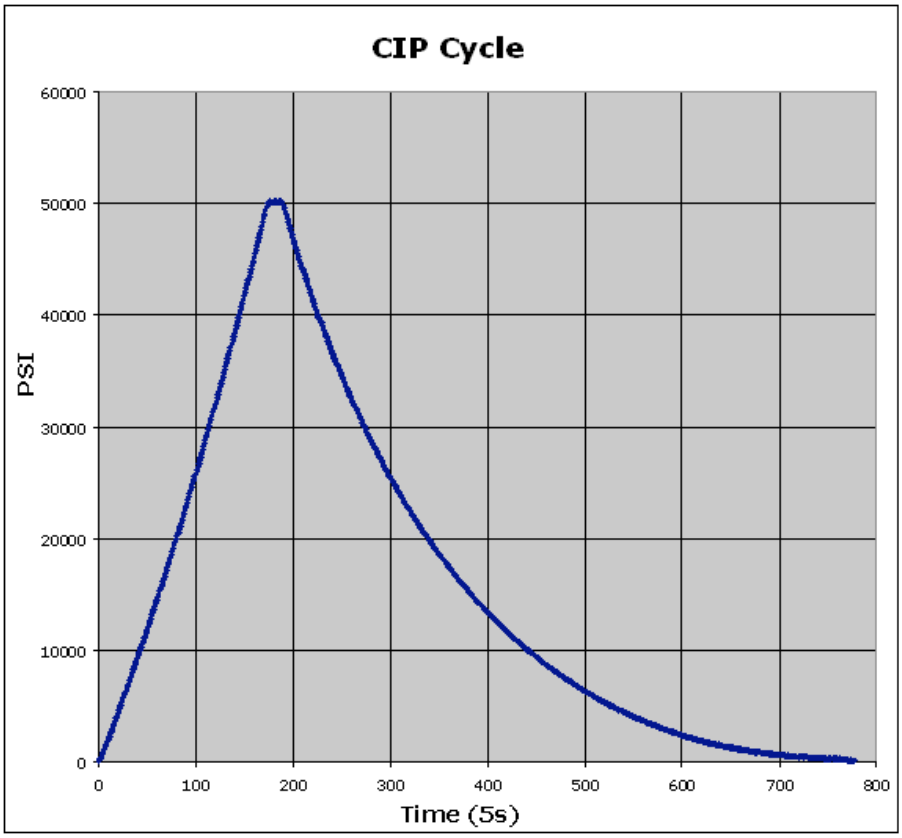

Fig. 3. CIP pressure cycle.

Upon completion of the CIP cycle, the cans were removed, dried, and then returned to an argon filled glove bag for further handling. Samples were removed from the CIP bag, sealed in Ziploc bags, and wrapped in bubble wrap for shipment.

CHAPTER IV

CIP RESULTS

The diametric compression of the samples varied widely, ranging from .250” to .023”. Further examination revealed the presence of cotton and plastic fibers along with other contaminates. In total, 22 rods were obtained via the CIP method. Two CIP bags (Samples 8a and 9a) ruptured during the third cycle and the contents were lost. Until these bags ruptured, the same six CIP bags were used for each cycle. After the rupture, three new bags were ordered and used for the remaining two cycles. Table 4 gives the initial sample dimensions as well as the final lengths and maximum diameters. The difference between the initial diameter and the final maximum diameter are also listed.

As is shown in the table below, samples 6, 6a, 7, and 7a had the least compression of any sample. Upon receipt, sample 6a crumbled and returned to powder. Samples 6, 7, and 7a were fragile and are crumbling, as well.

Samples 10 and 10a were by far the most rigid samples after the CIP. These also had the greatest reduction in diameter, and were the only samples that were free of yttrium. Generally, the samples with a greater decrease in maximum diameter were found to be more rigid and easily handled than the samples which experienced only a slight decrease in maximum diameter.

TABLE IV
CIP Sample Dimensions

Sample #	Initial Diameter (in)	Initial Length (in)	Max Final Diameter (in)	Final Length (in)	Absolute Decrease in Diameter (in)	% Decrease in Diameter
1	1.25	4.00	1.158	3.830	0.092	7.36
2	1.25	4.00	1.160	3.886	0.090	7.20
3	1.25	4.00	1.086	3.374	0.164	13.12
4	1.25	4.00	1.142	3.809	0.108	8.64
5	1.25	4.00	1.168	3.784	0.082	6.56
6	1.25	4.00	1.199	3.933	0.051	4.08
7	1.25	4.00	1.207	4.009	0.043	3.44
8	1.25	4.00	1.176	3.967	0.074	5.92
9	1.25	4.00	1.175	3.714	0.075	6.00
10	1.25	4.00	0.999	3.220	0.251	20.08
11	1.25	4.00	1.17	3.793	0.080	6.40
12	1.25	4.00	1.176	3.722	0.074	5.92
1a	1.25	<4.00	1.183	3.089	0.067	5.36
2a	1.25	4.00	1.177	3.327	0.073	5.84
3a	1.25	4.00	1.095	3.537	0.155	12.40
4a	1.25	<4.00	1.174	3.529	0.076	6.08
5a	1.25	<4.00	1.182	3.395	0.068	5.44
6a	1.25	4.00	1.227	3.053	0.023	1.84
7a	1.25	<4.00	1.225	3.436	0.025	2.00
8a	1.25	4.00	**Bag Rupture			
9a	1.25	4.00	**Bag Rupture			
10a	1.25	4.00	0.998	3.292	0.252	20.16
11a	1.25	<4.00	1.200	3.509	0.050	4.00
12a	1.25	<4.00	1.187	3.013	0.063	5.04

Microscopy and analysis

Optical microscopy

Excess trimmings off the ends of the CIP samples were analyzed under an optical microscope. Figures 4 and 5 show fibers embedded within the Nb. Due to the white color, and the fact that these fibers are located in the excess trimmings from the ends of the CIP samples, they are most likely due to the cotton filter used during the CIP process, as described previously.

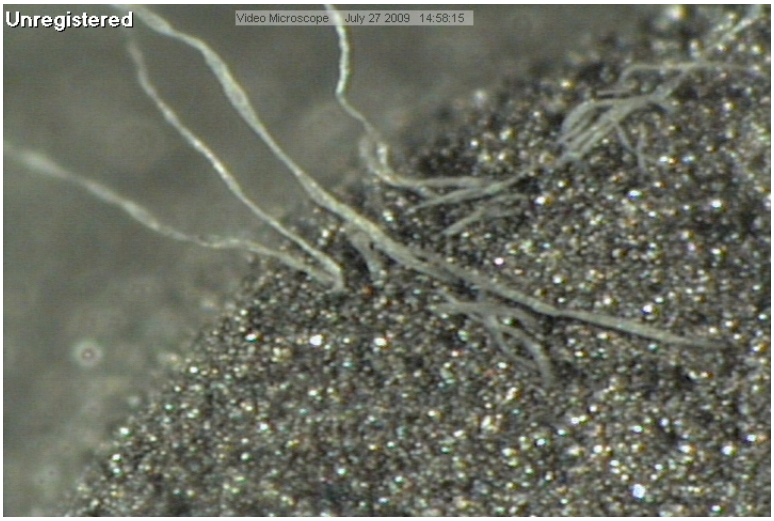

Fig. 4. Fibers embedded in Nb bulk.

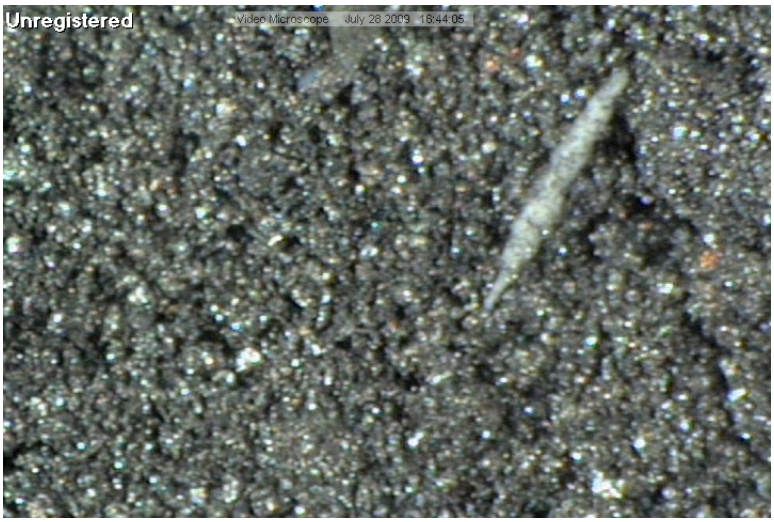

Fig. 5. White fiber embedded in excess trimmings.

Scanning electron microscopy (SEM)

SEM was performed by Kyle Damborsky of the Magnet Lab at Texas A&M University. The excess trimmings from the ends of the CIP samples, as well as trimmings from the bulk of several of the samples were analyzed. Figure 6 shows a fiber embedded in the bulk of sample 2. Figure 7 shows a fiber in the bulk sample 2 where the indicated regions appeared to melt under the high intensity electron beam. The fact that the fiber appeared to melt, coupled with its smooth texture compared to the cotton fibers, suggests that the fiber in Figures 5 and 6 is plastic in nature. This could have been introduced into the sample during the high energy blending of the powders prior to CIP. Due to the abrasive nature of many of the powders, small ribbons of plastic may have been torn off during the high energy blending of the powders in the high density plastic bottles. Based on the nature of their introduction, it can be assumed that these plastic ribbons would be distributed throughout the samples.

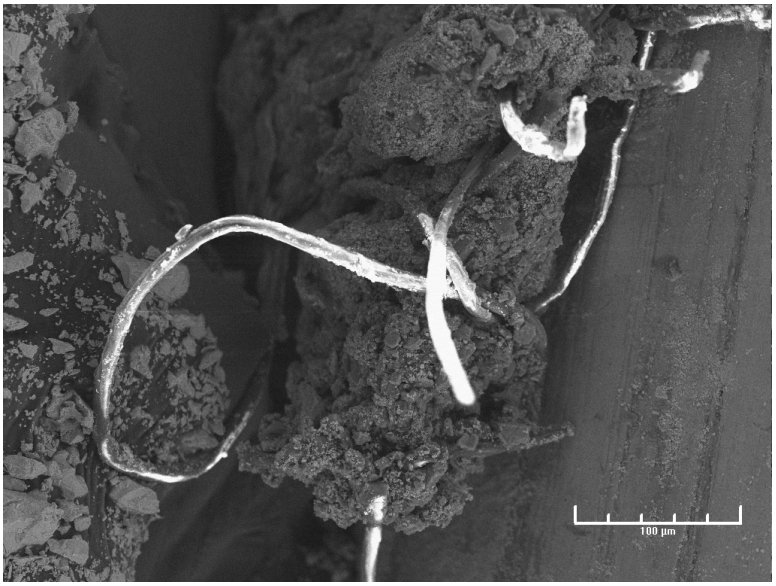

Fig. 6. Embedded fiber found in bulk of sample 2.

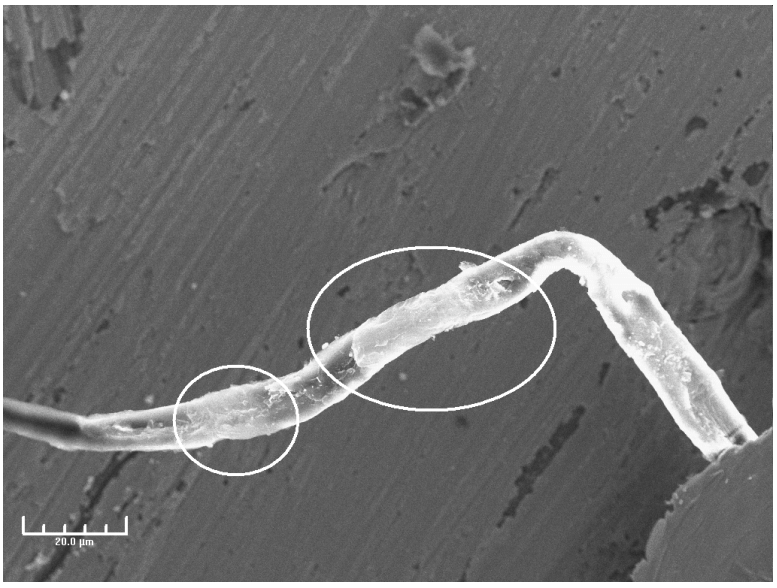

Fig. 7. Fiber in bulk of sample 2. Circled regions appeared to melt under the high intensity electron beam.

Energy dispersive spectroscopy (EDS)

EDS of the fibers mentioned above was performed by Kyle Damborsky of the Magnet Lab at Texas A&M University. Figure 8 shows the EDS spectra of a fiber found in sample 2 and Table 5 shows the weight percent of elements found in the sample.

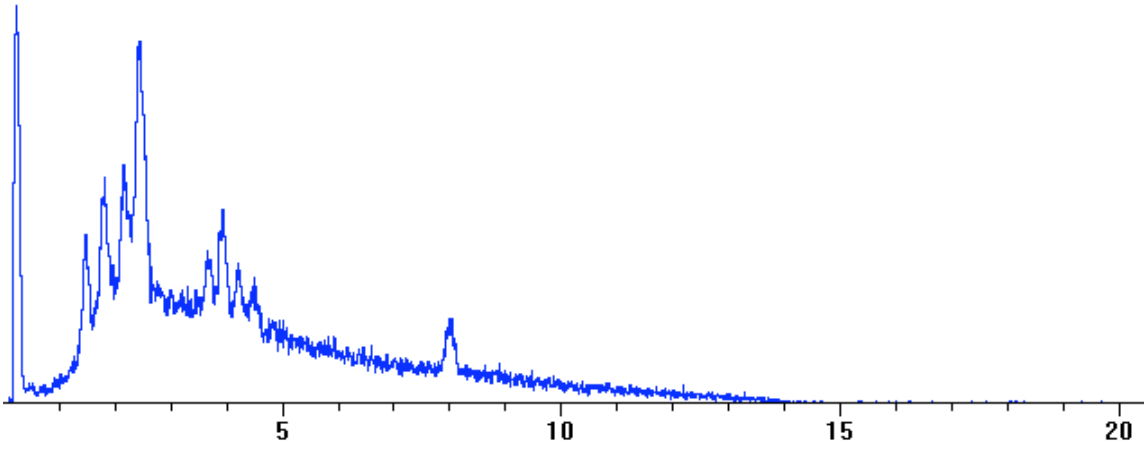

Fig. 8. EDS spectra of fiber found in sample.

TABLE V
Weight Percent of Elements

Element	Weight Percent
C	58.99
Al	1.88
Cl	0.00
Ca	1.87
Cu	14.32
Sr	6.30
Nb	6.44
I	9.21
Ti	0.99
Total	**100.00**

In general, the main impurity was carbon. During the acquisition of the spectra, flakes of powder were observed to cling to the sample under examination due to electrostatic interactions. Because of this effect, the elemental composition of the spectrum is difficult to determine accurately. Furthermore, it is not possible to distinguish hydrogen with EDS. While EDS was capable of determining the elemental composition of the impurities in the samples, the method lacked the sensitivity to distinguish between various hydrocarbons. The images of the impurities are therefore a much more useful tool in identifying the composition for the present case.

Aside from the expected elements (Nb, Y, W, Ti, Cu, and Zr), the elements Sr, Ca, I, Al, Pd, Cl, Au, Si, and Br were all possibly included in the material. The sample mounts were comprised of Al, and previous use of the sample mounts included coating with Au and Pd. The appearance of these elements can be attributed to the sample mounts. Sr an Ca appeared in trace quantities only (less that 1% of the sample region by mass), and are likely the result of cross contamination with Bi-2212 when handled in the glove box. Br appeared only in one sample and may be a misidentification of Zr or Y. Silicon also appears as a possible impurity, but due to the small amount included in the sample, Si and W are nearly impossible to distinguish. The origin of the I and Cl impurities is an unresolved issue.

CHAPTER V

PROBLEM SUMMARY

Optical and electron microscopy showed the presence of embedded fibers in the CIP samples. Plastic contamination is attributed to the high energy blending of the powders prior to CIP. Cotton contamination is attributed to the filter used during the evacuation of the CIP bags. Plastic fibers may be prevalent throughout the bulk of the samples, while the cotton fibers should be localized to the ends of the rods nearest the filter.

The fragility of many of the samples, as well as the return to powder of sample 6a may have been caused by several factors. The CIP cycles were not optimized based on materials used and the geometry of the cans. Due to the different volumes of the shorter samples, and the different materials used, identical CIP cycles would not work the same for all samples. Additionally, the high oxygen content of the Nb powder may have contributed to the lack of consolidation. With the surface of the Nb particles oxidized, the ductility and malleability of the powder particles decreases significantly. This can prevent the individual particles from metallurgically bonding during CIP, which, in turn, can prevent the sample as a whole from consolidating. Another effect of the high oxygen content of the Nb powder would be the decreased performance of the Nb_3Sn superconductor. Therefore, low oxygen content Nb powder must be produced for the successful production of Nb_3Sn superconductor. Two methods of powder production are discussed in the following section.

CHAPTER VI

Nb POWDER PRODUCTION

Two methods of obtaining low oxygen content Nb powder were investigated. The first is a method of production, where the powder is manufactured by SPD. The second method utilizes commercially available Nb powder and an inductively couple plasma (ICP) torch to remove the oxygen from the surface of the powder particles.

Severe plastic deformation

The SPD method utilizes a roughing cutter on a mill to machine a Nb plate. After the outer layer of Nb is machined off, the bulk Nb will have a low oxygen content. Ideally, the process can be done in an Ar atmosphere, preventing the oxidation of the remaining Nb. Previous studies have used a lathe and a piezoelectric cutter to machine other materials, resulting in chips with sizes in the range of 100-200 micrometers [10]. Using a lathe proved to produce too low of a yield, so a roughing cutter on an end mill was utilized. As opposed to a cutter on a lathe, a roughing cutter for a mill has many points of contact along each cutting edge, as well as multiple cutting edges. This enables the roughing cutter to produce a larger number of chips, as well as smaller chip sizes, than a conventional cutter. The cutter that was used in this project was a 3/8” diameter, fine pitch roughing cutter with 4 flutes. A picture of the roughing cutter is shown in Figure 9.

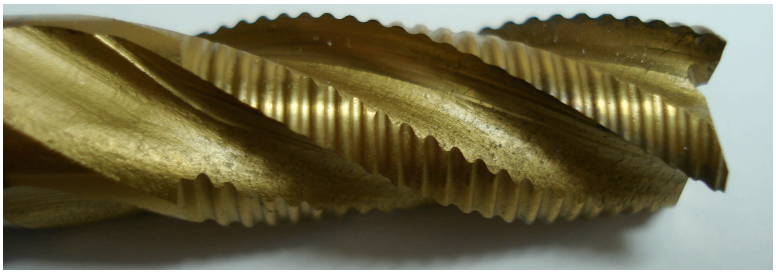

Fig. 9. Cutting tool for Nb chip formation.

By varying the tool speed, the feed speed, and the cutting depth, we were able to produce chips in the size range of 100-300 micrometer range. The chips were rectangular in shape. A picture of a sample of chips is shown in Figure 10. The initial chip forming design was to secure a glove bag around the bed of the mill, with a rotary shaft seal around the tool collet, to keep the Nb in an Ar atmosphere. However, previous work has shown that even in a high purity 99.98% Ar atmosphere, Nb undergoes significant oxidation [11]. Additionally, a plastic glove bag would be permeable to water vapor, allowing an oxygen source to enter the process. For this method to have a chance of working, a glass enclosure with a recirculator to remove water vapor and 99.999% pure Ar would have to be used. Even then, problems with oils on the mill outgassing would lead to possible impurities in the Nb powder. All of these issues led us to cancel production of powder by this method.

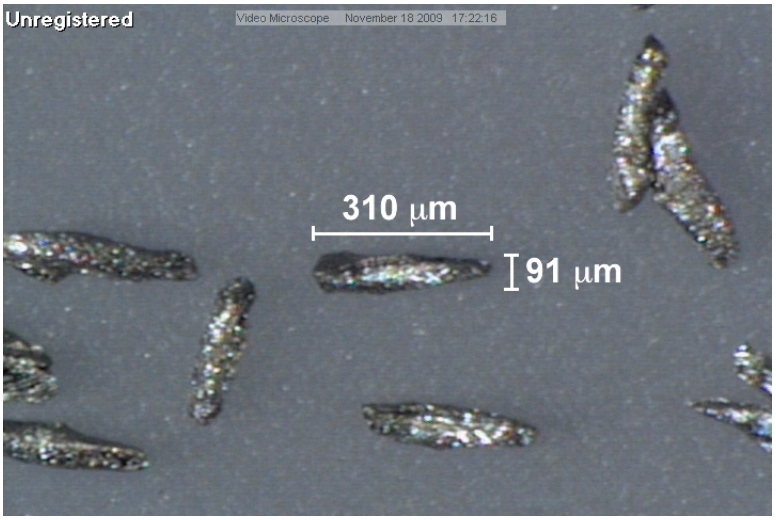

Fig. 10. Nb chip formed by SPD.

Inductively coupled plasma torch

The ICP method is a refining method instead of a manufacturing method, although a DC torch can be used to create powder from bulk Nb. Commercially available Nb powder, with high oxygen content, can be refined with an ICP torch in such a way that the oxygen content is lowered. The powders are put through an ICP torch with a gas that is comprised of argon with a small amount of hydrogen to remove the oxygen [12]. This process is mainly done by Tekna Plasma Systems, an industrial plasma torch company that is based in Quebec, Canada. By personal communication with Tekna Plasma Systems, we know that they have not processed Nb powder, but they have processed tantalum, which has very similar chemical properties as Nb. With the Ta, Tekna saw a total reduction in oxygen content by a factor of two after processing with one pass through the ICP torch and packaging. Tekna estimates that the maximum decrease in oxygen content for Nb would be by a factor of 10 if all parameters are optimized. A

decrease by a factor of 10 would enable us to reduce the oxygen content in our Nb powder from 3000 ppm to 300 ppm in one pass, and to 30 ppm in two passes.

This method has a high initial cost, which makes it expensive at the research level. However, at the industrial scale of Nb powder production, the system can output upwards of 100 kg per hour, which would make the cost per kg of powder low enough for industrial scale production. Due to this high initial cost, the powder has not yet been produced, although negotiations are currently taking place for the production of several kg of low oxygen content Nb powder for use in a proof of concept experiment.

CHAPTER VII

CONCLUSION OF Nb3Sn PROJECT

Powder metallurgy, specifically CIP and HIP, has the potential to be used for the placement of artificial pinning centers. The main issue is the low oxygen content that is required for the Nb powder. If Nb powder with low enough oxygen content can be manufactured, the process that we have discussed could be used to disperse candidate materials in the Nb powder to act as pinning sites. Instead of high energy blending, which introduced contaminants, a jet mill can be utilized to mix the powders. The CIP was shown to produce rods, and with a HIP process to follow, a solid billet can be achieved. The changes in the mechanical properties of the material are still unknown, as is the change in pinning force. Utilizing an ICP torch to produce low oxygen content Nb powder, and a jet mill to mix the powders, a second attempt can be done to determine if it is possible to see an increased performance of Nb_3Sn superconducting wire.

CHAPTER VIII

INTRODUCTION TO Bi-2212 PROJECT

The objective of this project is to develop a method to magnetically texture Bi-2212 powder for use in a modified jellyroll (MJR) round wire production. Bi-2212 is a ceramic high temperature superconductor with a critical temperature of 95K, which has been shown to carry current in magnetic fields as high as 45 Tesla [13]. The performance of Bi-2212 round wire compared to other superconductors in high magnetic fields can be seen in Figure 11 [13]. However, the critical current density of Bi-2212 at high fields is significantly smaller than necessary for Bi-2212 to be practically used in accelerator quality magnets.

The crystal structure of the material, as shown in Figure 12 [14], is such that the bulk of the current carrying capacity in Bi-2212 is in the a-b plane [15]. The a-b plane is the plane consisting of the CuO_2 molecules. This project utilizes a magnetic texturing technique to align the powder particles in such a way that the a-b planes of different particles are aligned. This will, in turn, enhance the J_c of wires made of the material.

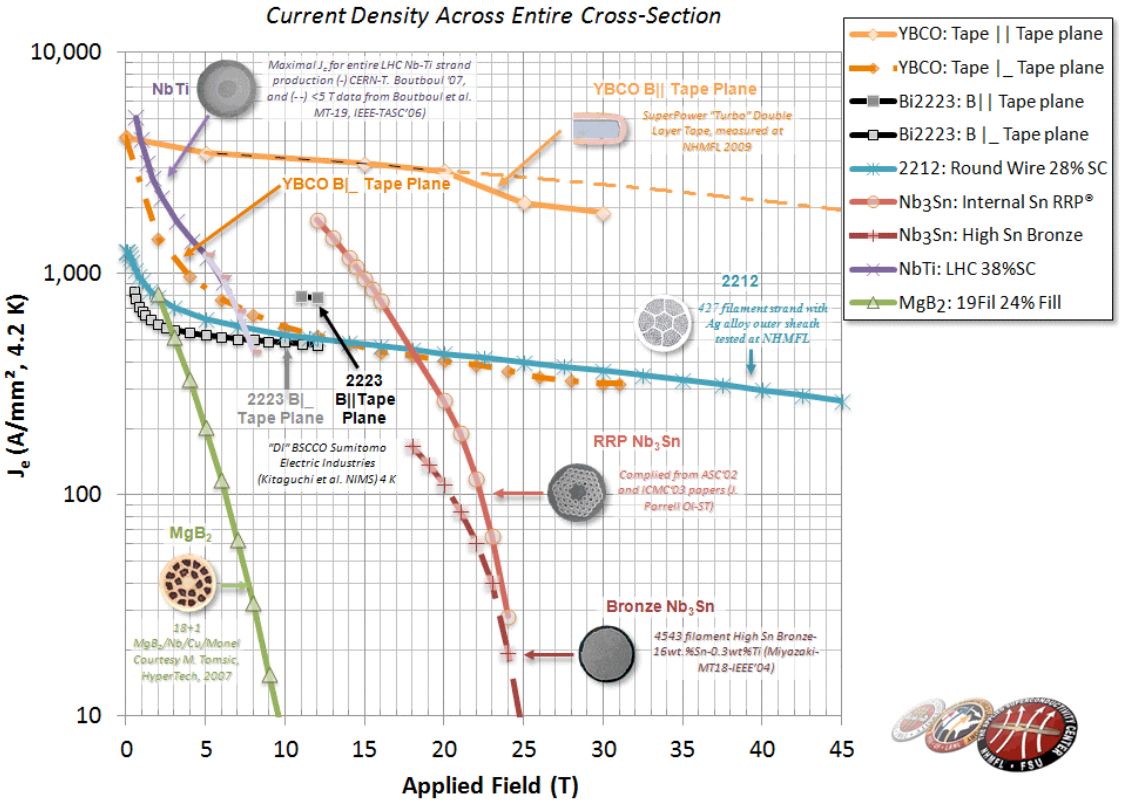

Fig. 11. J_c vs. B for different superconductors.

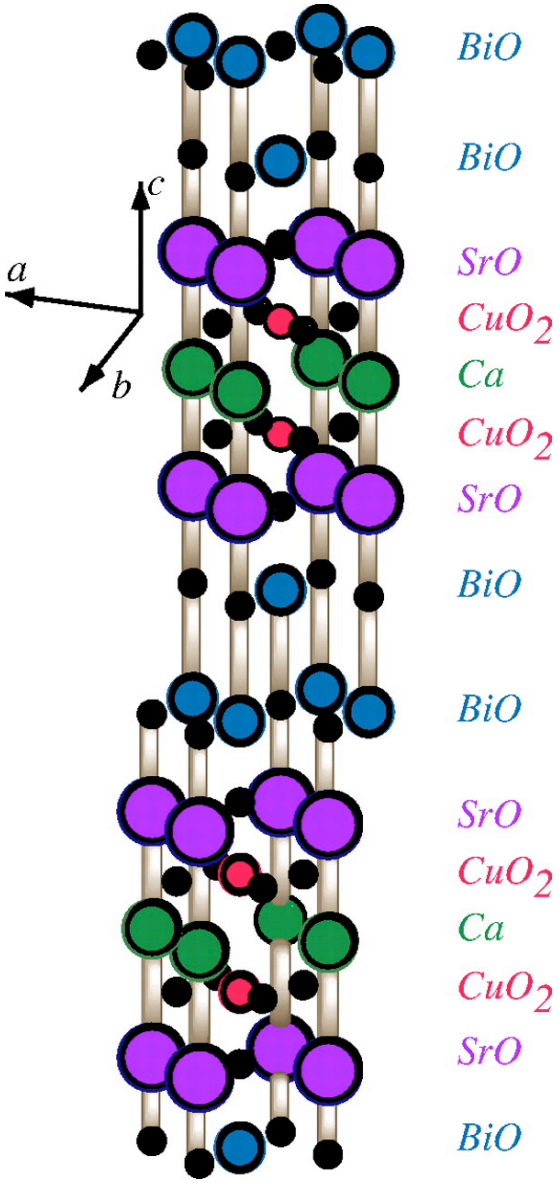

Fig. 12. Crystal Structure of Bi-2212.

Previous research was conducted in the summer of 2009 using a slow curing epoxy to suspend Bi-2212 powder while in the presence of a magnetic field of 8.9 T. The X-ray diffraction (XRD) data suggests that the individual powder particles were aligned. The (0,0,8) peak is a c-axis peak, and (2,0,0) is an a-axis and b-axis peak, since they are

symmetric. Figure 13 shows the ratio of the c-axis to the a,b-axes peaks. The ratio increases with time left in the field, which illustrates how the c-axis of the crystal becomes the predominant orthogonal axis. This implies that the a-b plane is the predominant plane in the sample. The magnetic field is attributed with suppressing the a-axis and b-axis from aligning with the magnetic field.

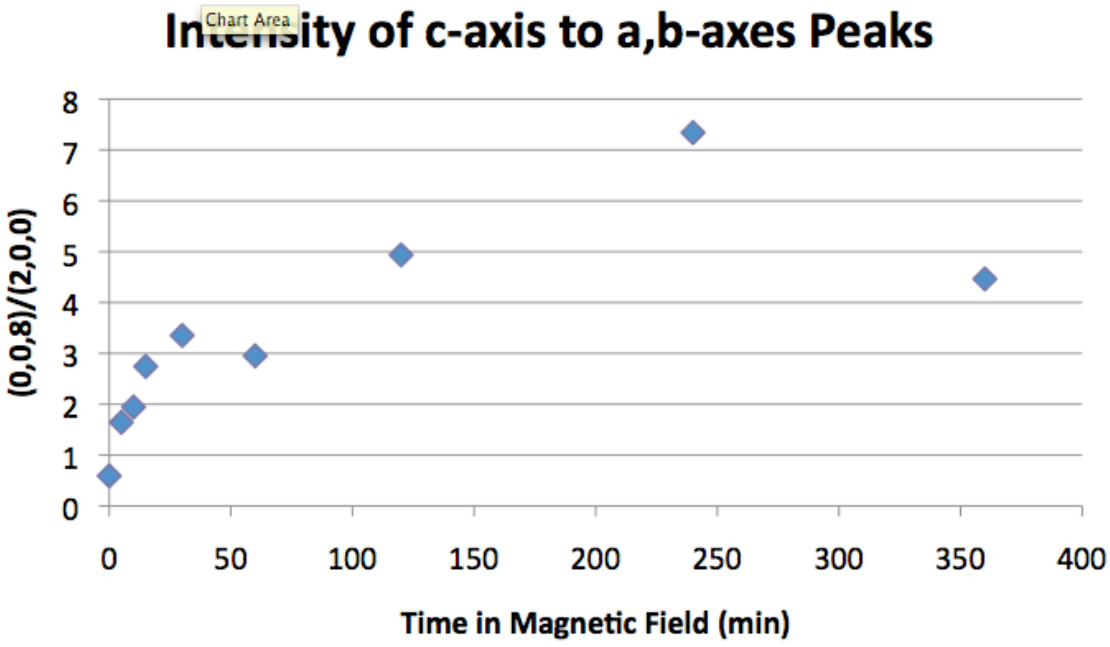

Fig. 13. Intensity of c-axis peaks for powder in a slow curing epoxy.

We further develop this technique by suspending the powder in a solvent, placing the solvent with a submerged aluminum substrate in a magnetic field, and evaporating the solvent. We begin our study with three different solvents – ethanol (EtOH), isopropyl alcohol, and methanol (MeOH) – but our discussion focuses on the use of EtOH. We begin with residual gas analysis (RGA) and trace analysis of the evaporated solvents to

determine whether the solvent evaporates cleanly. We then check whether ultrasonic vibrations decrease the particle size, and if this has any effect on the deposition of a layer of powder on the Al substrate. The final step is a magnetic orientation test where the powder is evaporated on an Al substrate in a magnetic field.

The powder would be used in a MJR round wire production method. This method entails magnetically texturing the powder on a silver alloy foil substrate, extrusion, and heat treatment to form the round wire. The manufacturing process is discussed in more detail below.

The order of this section is as follows. We will first discuss the wire production method. Second, the materials and methods used in this experiment are presented. Next, we analyze and discuss the results of the experiments. We will then conclude with the status of this project and the future plans.

CHAPTER IX

WIRE PRODUCTION

The goal of this project is to develop a method to magnetically texture Bi-2212 powder for use in a MJR method for round wire production. This method would entail magnetically texturing the powder in corrugated channels on a silver or silver alloy sheet. The sheet would then be rolled up such that all of the powder particles are oriented in the proper way. The rolled up sheet of silver alloy and Bi-2212 would then be extruded into a rod. Nineteen rods would then be stacked atop each other, and sheathed in a silver-magnesium tube. This would then be extruded into another rod, and nineteen of the jelly-roll elements will be restacked and sheathed and extruded again. This will produce ~1 km of 1.0 mm diameter round wire. A drawing of the entire process can be seen in Figure 14. After the round wire is formed, it is wound into Rutherford cables, which are used in magnet production. The final step is a heat treatment to consolidate the Bi-2212 powder and produce a well connected conductor.

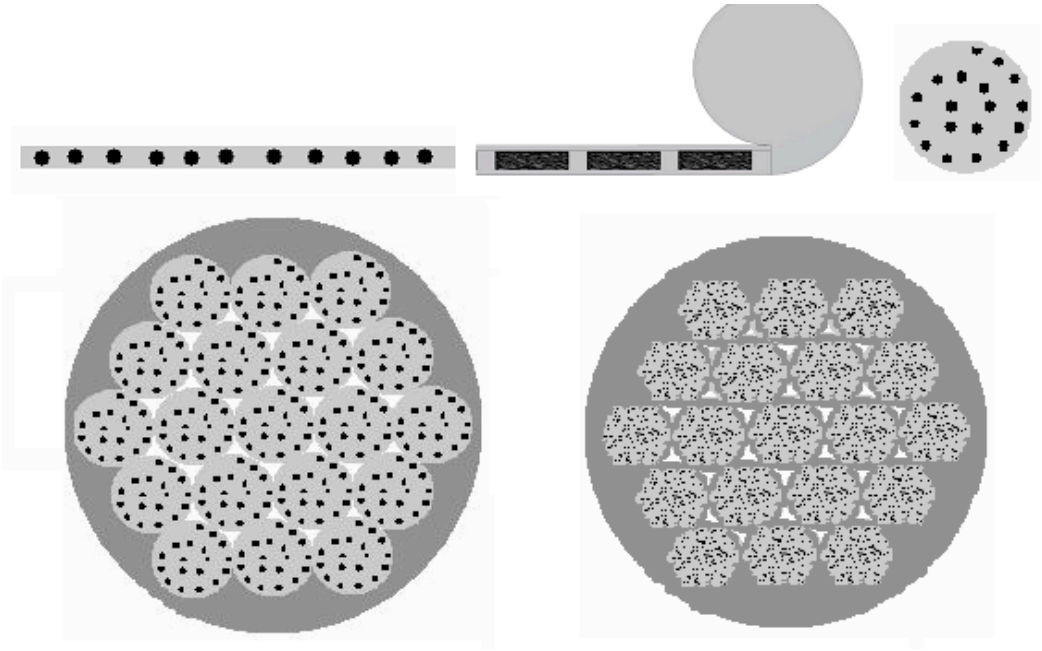

Fig. 14. MJR wire production process.

CHAPTER X

MATERIALS AND METHODS OF Bi-2212 PROJECT

For the evaporation and magnetic orientation tests, three solvents were tested. EtOH, isopropyl alcohol, and MeOH were all used in individual tests. For the ultrasonic vibrations tests, only EtOH was used as a solvent.

Evaporation tests

For the evaporation tests, three trials were run – one for each solvent. 10.0 mL of the solvent was mixed with 40.0 mg of Bi-2212 powder in plastic container. The solution was then shaken by hand for one minute, and a syringe was used to draw 4.0 mL off the top of the solution, and deposited into a test tube, with a pure Al SEM sample mount as a substrate. The test tube is then connected to a vacuum pump with a rubber stopper that has a through hole. The vacuum is brought down to -29 in Hg (~2000 μm Hg) until the alcohol in the solution is fully evaporated and only powder remains in the test tube, at which time the pressure of the system reaches ~50 μm Hg. A picture of the evaporation test set up is shown in Figure 15.

Fig. 15. Evaporation rig.

Ultrasonic vibration tests

For the ultrasonic vibration tests, 4.0 mg of Bi-2212 powder with mixed with 4.0 mL of EtOH in a test tube. The test tube was then placed in the water bath of an ultrasonic cleaner, and vibrated for 1 min, 5 min, and 10 min. A calibration test was done in which the solution was shaken by hand for 1 min. An Al substrate was then inserted into the test tube, and the test tube was connected to the vacuum pump used in the evaporation test. The solution was then evaporated in the same manner as in the evaporation tests. The substrates were then removed from the test tube and analyzed by SEM.

For the ultrasonic vibration tests, the powder and EtOH were put directly in the test tube, and a syringe was not used. This is different from the evaporation tests, where a syringe was used to draw from the top of the solution.

Magnetic orientation tests

For the magnetic orientation of the Bi-2212 powder, a solution of 40 mg Bi-2212 powder mixed with 10 mL EtOH was used. The solution was shaken by hand for 1 min and 4 mL were drawn from the top with a syringe. The solution was inserted into a fixture that was inserted into an 8.9 T magnet. The fixture was built by Andrew Jaisle of the Texas A&M Magnet Lab and comprised of nonmagnetic components. It consisted of a long aluminum tube that protruded from the magnet, and a sample mount holder at the bottom of the fixture. After being inserted into the fixture, the top of the tube was connected to a vacuum pump, which evaporated the solution until a change in the pressure was noted (from ~2000 μm Hg to 200 μm Hg). This was between two and three hours for the EtOH and isopropyl samples, but the MeOH was allowed to evaporate overnight. The fixture was then removed from the magnet and the sample mount was analyzed.

CHAPTER XI

RESULTS

Evaporation tests

Due to the ultrasonic vibration and magnetic orientation tests being conducted with EtOH only, we will focus on the EtOH test of the evaporation test, as well. During the evaporation tests, an issue that initially arose was the violent bubbling of the solution as the pressure was suddenly decreased. While at first this was believed to be due to the boiling point of the alcohol decreasing as the pressure is decreased, it was soon realized to be due to an air pocket that becomes stuck under the Al substrate in the test tube. The violent bubbling of the solution would cause the powder to be disturbed, and a layer of powder would not be properly deposited on the substrate. This is not an issue that will arise in the final production state of the process, when the powder solution is on the silver alloy substrate, since there will be no space for an air pocket to become trapped. However, for our testing purposes, this proved to be an issue. We resolved this issue by decreasing the pressure slowly over a period of 10-20 minutes, in which time the air pocket would decrease in size with small bubbles rising on the sides, as opposed to violent bubbling of the solution. After the pressure was slowly brought down, and the air pocket was diminished, the vacuum was brought to a full vacuum of -29 in Hg.

A calibration test was done on the RGA with an Al substrate and either pure EtOH, MeOH, or isopropyl alcohol. After running an evaporation test with EtOH, RGA

showed no contamination of the Bi-2212 powder with EtOH. The RGA results are shown below, in Figure 16. As the graph shows, there is no peak at 46 amu, which is the molecular mass of EtOH.

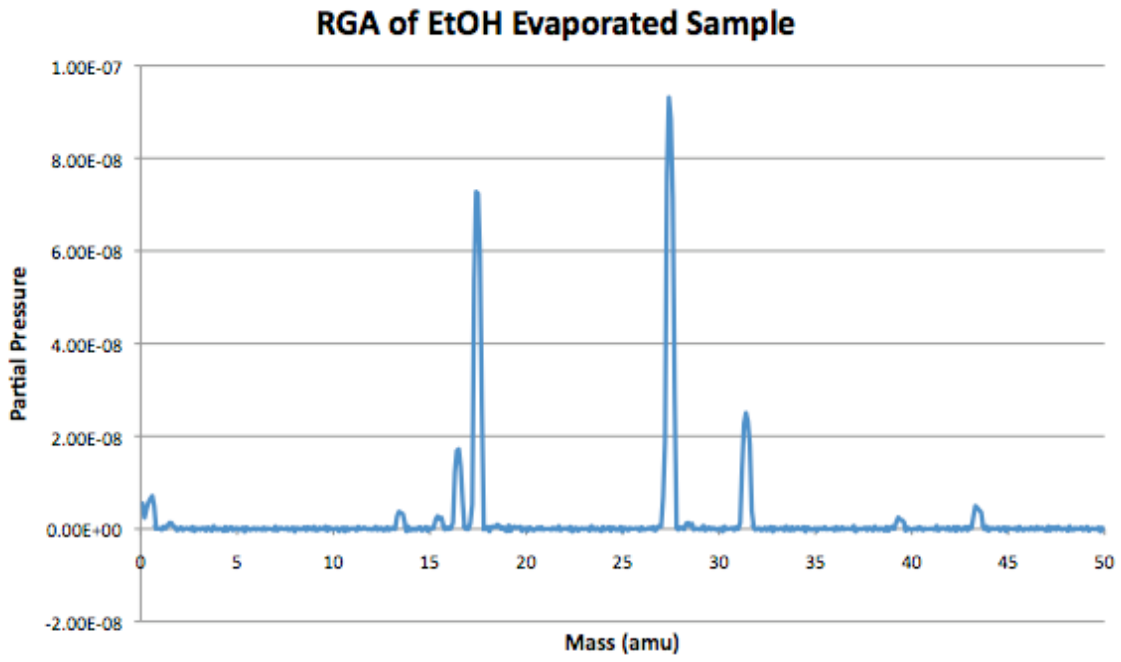

Fig. 16. RGA of EtOH evaporated sample.

Even though the RGA showed that the EtOH evaporated cleanly, leaving no trace of EtOH on the Bi-2212 powder, trace analysis did reveal a large amount of carbon contamination. Trace analysis is conducted by bombarding the sample with oxygen ions, which eject other particles from the surface. The raw data is shown in Figure 17. Note that the ions of Sr and Ca are detected via their isotopes ^{84}Sr and ^{44}Ca, which are of low abundance. The signal of the most abundant isotopes is too high for this analysis.

CO is most likely from interactions between carbon and oxygen during the ionization. CaC could be a result of Ca ions and C ions interacting during the emission process. CaC is not necessarily present in the sample. The C_2H_3 is a hydrocarbon that could be from the solvent being adsorbed to the surface. It could also be from the pump oils. Note that the intensity is 3 orders of magnitude less than that of ^{44}Ca or ^{84}Sr. Even though the Bi-2212 is showing contamination, the C and H can be removed from the material through calcination, where the Bi-2212 is heated to 600-700^{o} C in a pure O_2 environment. Bi-2212 can handle the pure oxygen atmosphere, and C and H will interact with O_2 to form CO and H_2O gasses which may then be evacuated, either through a lamellar gas flow, or vacuum evacuation.

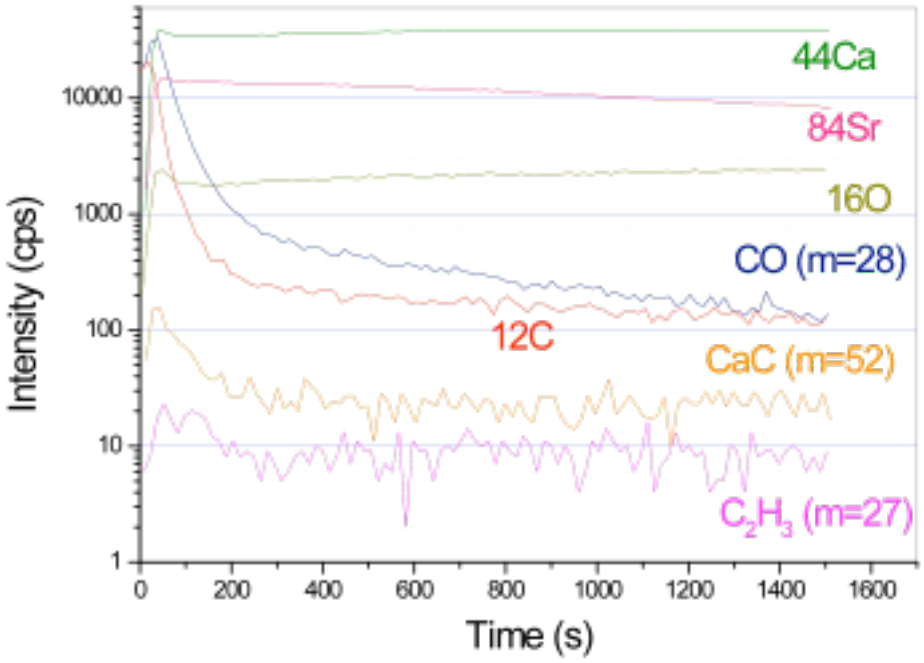

Fig. 17. Trace analysis of EtOH evaporated sample.

The SEM sample mounts that were used as substrates in the evaporation tests were analyzed by Kyle Damborsky, of the Texas A&M University Magnet Lab. The results of the SEM show a thin layer of powder deposited on the Al substrate. This can be seen in Figure 18.

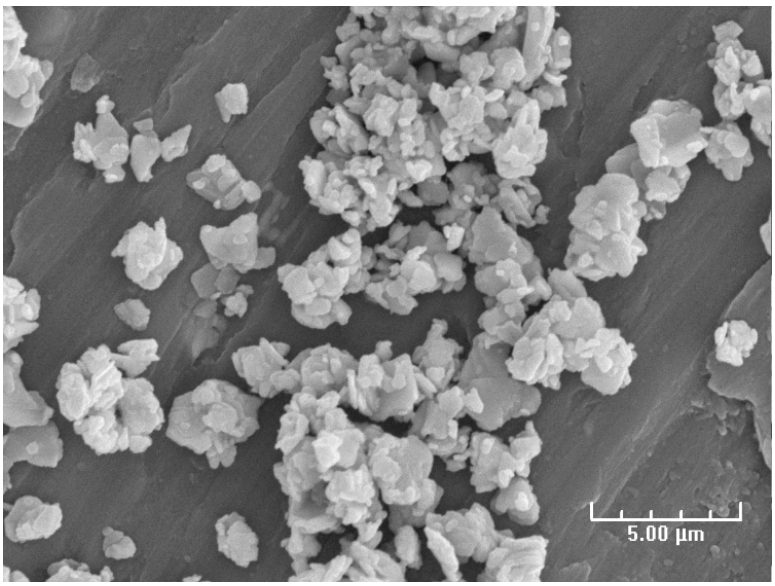

Fig. 18. Thin layer of powder deposited during evaporation test.

Ultrasonic vibration tests

For the 0 min ultrasonic vibration test, in which a syringe was not used, a uniform layer of powder was deposited on the surface of the substrate after evaporation. This sample had a significantly thicker layer than any of our previous trials. A large number of agglomerates was also observed. However, the large agglomerates were coated with a

layer of small agglomerates. This is illustrated in Figures 19 and 20. The thicker, more uniform layer can be attributed to the fact that since a syringe was not used to draw from the top of the solution, larger particles were in the solution. The powder also gathered at the edge of the sample mount, as is seen in Figure 21.

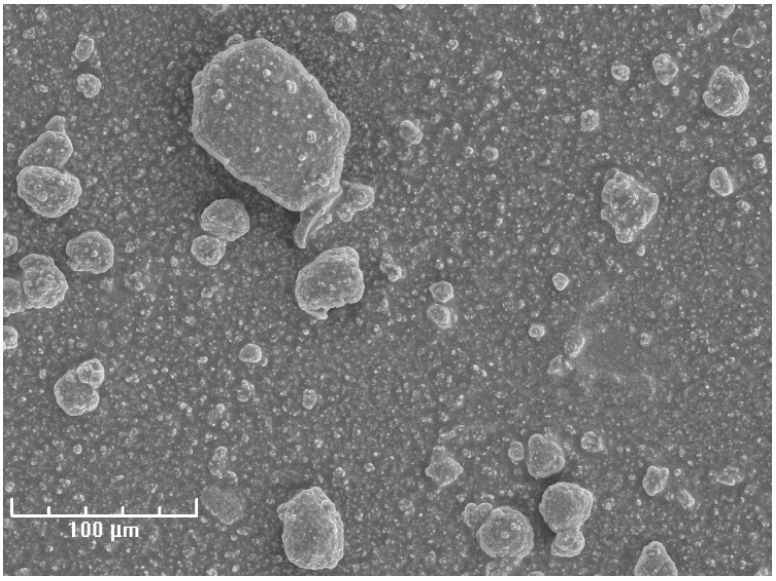

Fig. 19. 0 min, no draw.

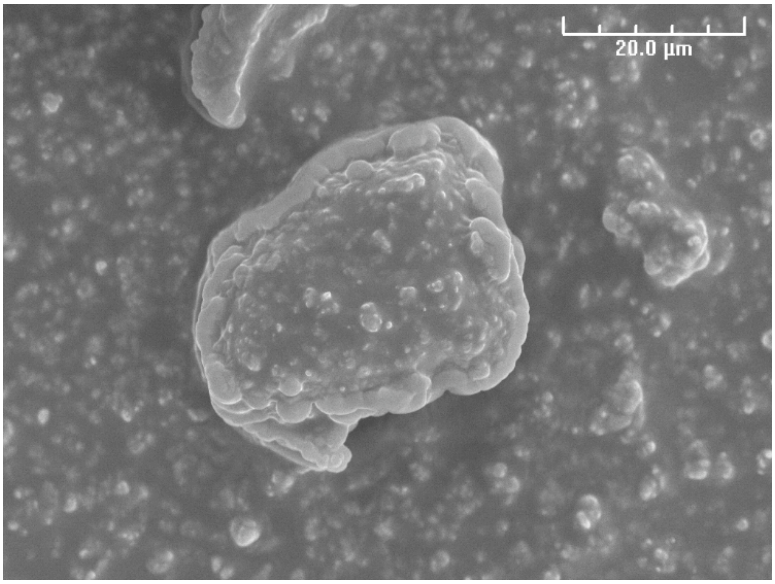

Fig. 20. Surface of agglomerate.

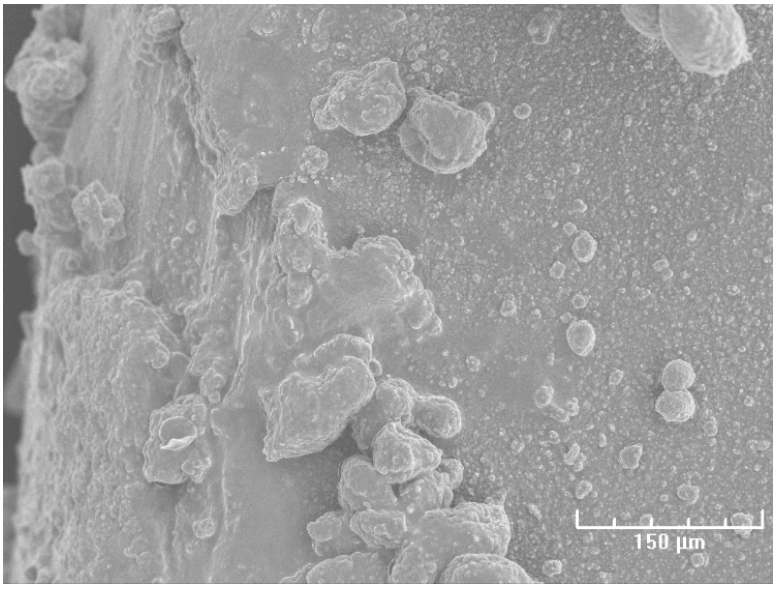

Fig. 21. Edge of sample mount.

For the ultrasonic vibration tests, a smaller particle size of the Bi-2212 powder was clearly observed. The powder was also suspended in the solution in a much more

uniform manner than by simply shaking the solutions by hand. In contrast to the 0 min test, the powder was only deposited on a portion of the substrate, and not on its entire surface. A possible cause of this is believed to be the fact that the substrate is not perfectly level in the test tube. Due to the base of the substrate being flat, and the bottom of the test tube being round, it is extremely difficult to obtain a flat surface once the substrate is inserted into the test tube. This uneven coating can be seen in Figure 22. However, the area where powder was deposited showed a very uniform layer of smaller particles (Figure 23). Compared to the samples that were not ultrasonically vibrated, a significant decrease in particle size was observed by ultrasonically vibrating the powder, with particle sizes of less than a micrometer obtained. This is shown in Figure 24. For the 1 min sample, agglomerates still remained, but for the 10 min sample, there were very few, as can be seen by comparing Figures 25 and 26.

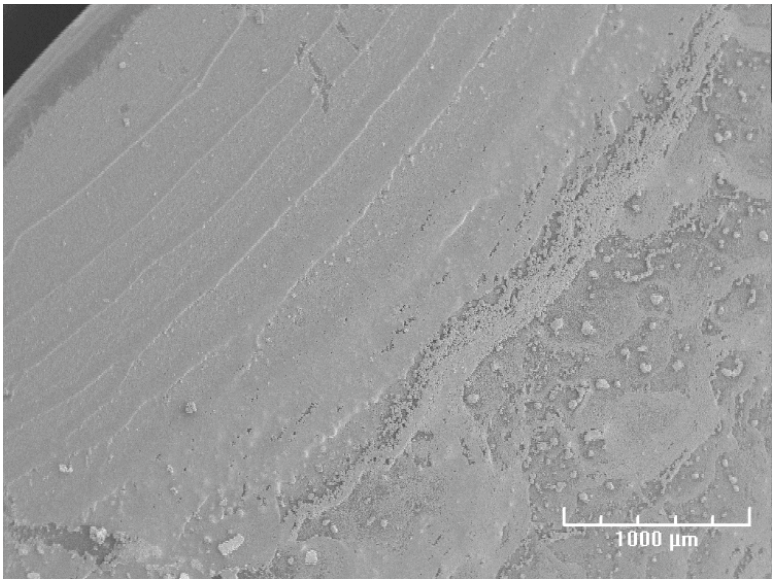

Fig. 22. 1 min ultrasonic with uneven coating.

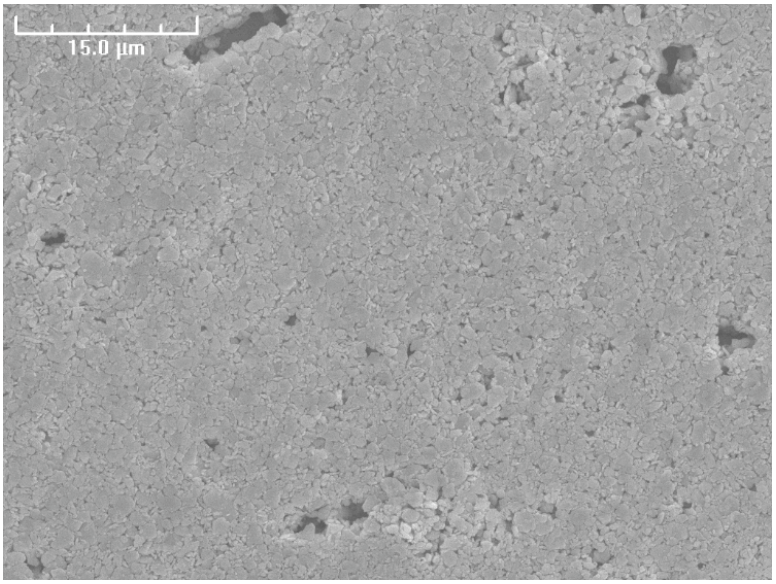

Fig. 23. 1 min ultrasonic with thin, even layer.

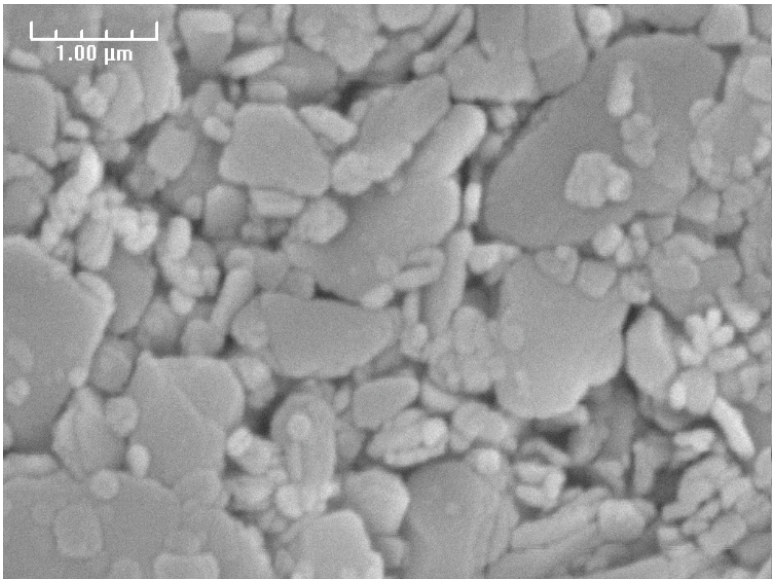

Fig. 24. 1 min ultrasonic with submicrometer particles.

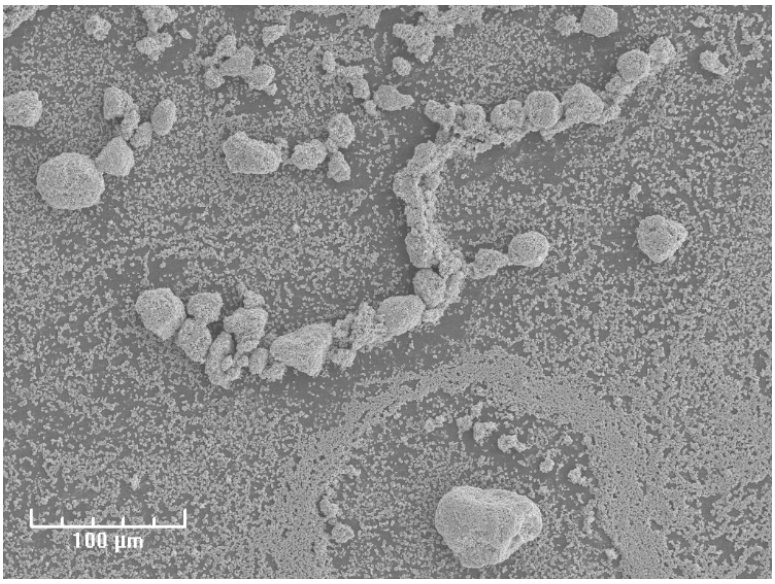

Fig. 25. 1 min ultrasonic with many agglomerates.

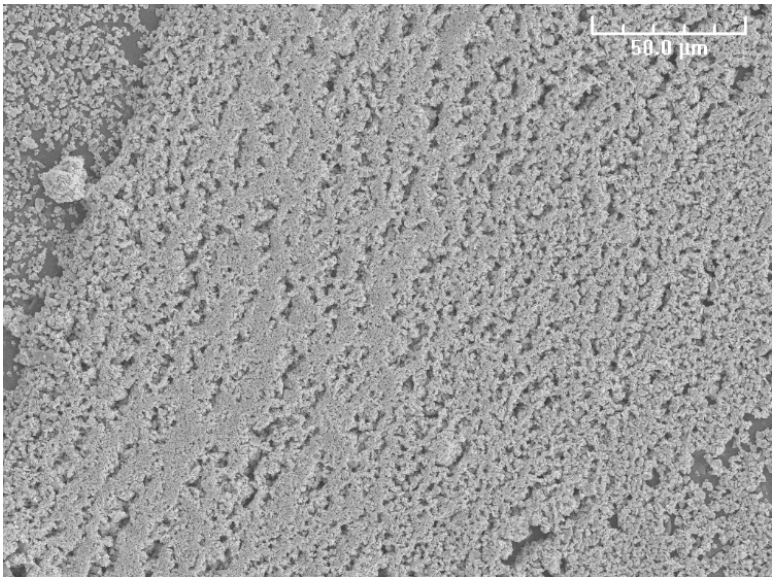

Fig. 26. 10 min ultrasonic with few agglomerates.

Magnetic orientation tests

Our magnetic orientation tests utilized SEM sample mounts that had indentations machined into them so that the powder would collect on the inside of these wells. We did observe a texturing of the powder, as is seen in Figure 27 (with magnetic orientation) compared to Figure 28 (without magnetic orientation). The XRD results are shown below in Figures 29 and 30. We did observe an increase in the orientation of the powder, although not as good as what was observed with the slow curing epoxy. MeOH showed a slightly better orientation than EtOH, but not significantly. Both showed a considerable increase over the sample that was not magnetically oriented.

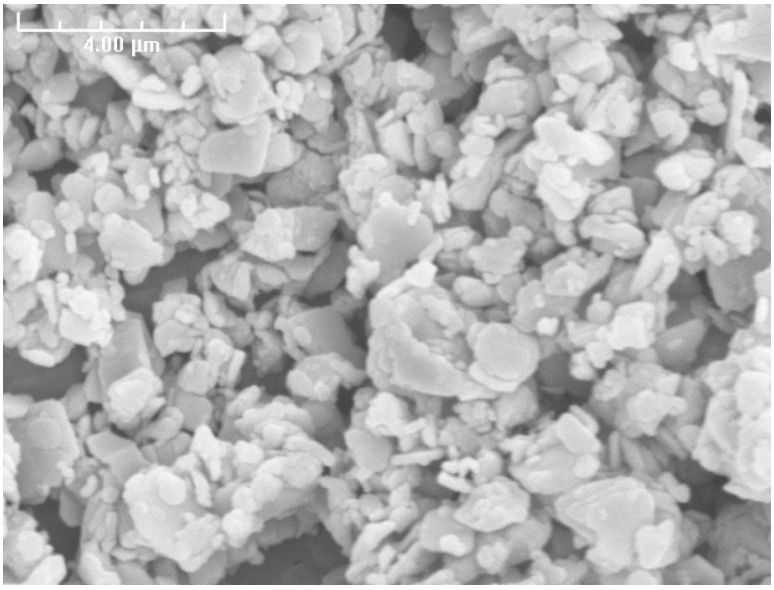

Fig. 27. Magnetically oriented Bi-2212 powder.

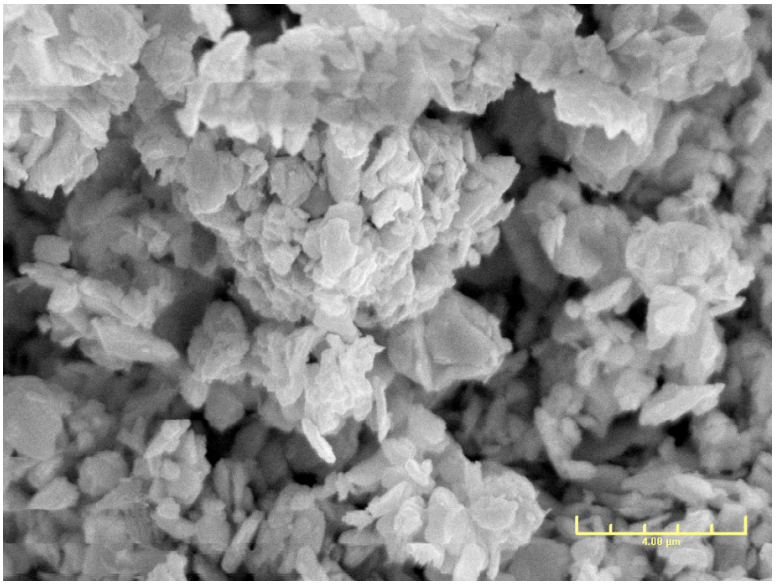

Fig. 28. Bi-2212 powder that has not been magnetically oriented.

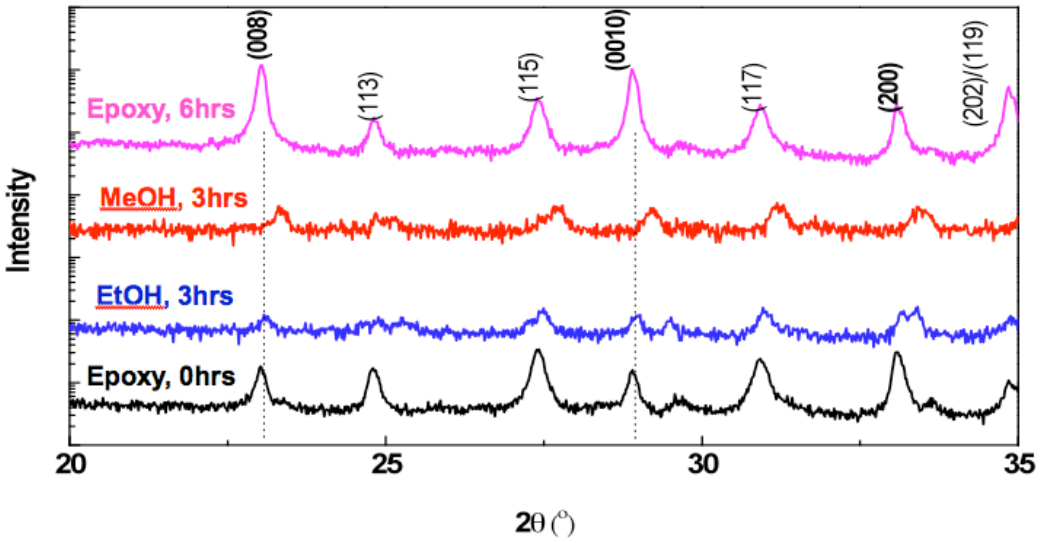

Fig. 29. Intensity of different peaks from XRD.

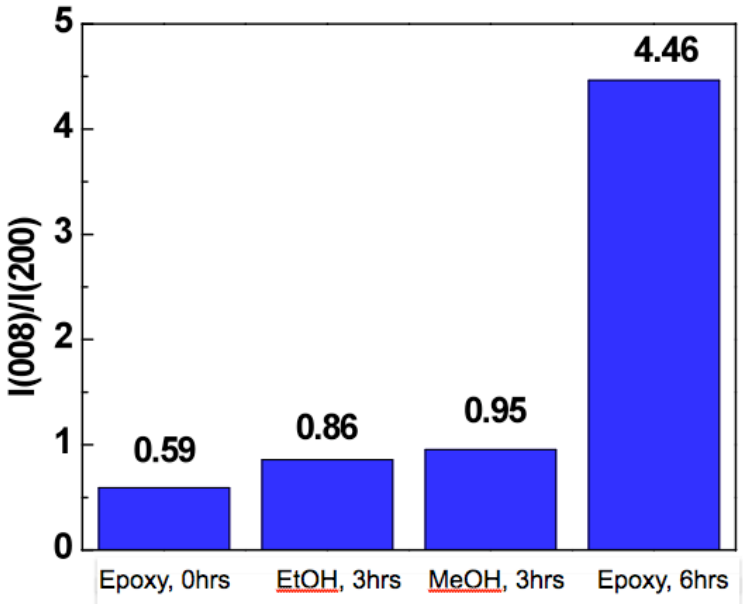

Fig. 30. Ratio of c-axis peaks to a,b-axes peaks.

CHAPTER XII

CONCLUSION OF Bi-2212 PROJECT

The evaporation tests, and the subsequent trace analysis showed a significant amount of carbon contamination in the Bi-2212 powder. This can prove to be an issue if EtOH is used in the final production method. An alternative solvent to use would be liquid argon. Liquid Ar has the benefit of being inert, and so, will not interact with the Bi-2212. Additionally, the magnetic susceptibility of Bi-2212 at liquid Ar temperature will enable a less powerful magnet to orient the powders. A less powerful magnet will cost less money to use, and will make the entire process more affordable and more readily controlled.

The ultrasonic vibration showed that the particles could be made significantly smaller. The ultrasonic vibrations were successful in breaking apart the larger agglomerates, leaving us with submicrometer particles. A difference between the 10 min and 1 min tests was also observed, which suggests that vibrating for longer periods of time will better enable us to obtain smaller particles.

Most importantly, the magnetic orientation tests showed that this process has the potential to orient the powder so that the crystal structure is coherent amongst the different particles. The benefits to the superconducting properties of the material are still to be determined. However, if there is an observed benefit in the superconducting

properties of Bi-2212, this process will prove to be a stepping-stone in the optimization of the Bi-2212 round wire production for use in superconducting magnets.

CHAPTER XIII

CONCLUSION

Superconducting round wires have the potential to be developed from both Nb_3Sn and Bi-2212 in a manner in which their properties are enhanced. The Nb_3Sn project has shown that the powder metallurgy methods described can be used to include nanoscale inclusions, which will act as artificial pinning sites. Although the oxygen content of Nb powder proved to be a limiting factor within the development of Nb_3Sn, the powder manufacturing techniques discussed can be used to combat this. Future plans include utilizing these methods in an additional attempt.

Utilizing an external magnetic field to orient Bi-2212 powder that is suspended in a solvent has proven to be a successful method of aligning the particles in the desired manner. Magnetic orientation of the particles has the potential to increase the current carrying capacity of round wires to what would be needed for high field magnets. Future plans include experimenting with other solvents in order to find one that will leave no residue, while still allowing the particles to be oriented.

Nb_3Sn and Bi-2212 still require significant development before the successful manufacturing of round wires, but the techniques developed for both materials have shown that the goals of optimized pinning in Nb_3Sn and an increased current carrying capacity of Bi-2212 are achievable.

REFERENCES

[1] A. Godeke, D. Cheng, D. R. Dietderich, P. Ferracin, S. O. Prestemon, G. Sabbi, and R. M. Scanlan, "Limits of NbTi and Nb3Sn, and development of W&R Bi–2212 high field accelerator magnets," *IEEE Trans. Appl. Superc.*, vol. 17, no.2, pp. 1149-1152, June 2007.

[2] J. Schwartz, T. Effio, X. Liu, Q.V. Le, A.L. Mbaruku, H.J. Schneider-Muntau, T. Shen, H. Song, U.P. Trociewitz, X. Wang, H.W. Weijers, "High field superconducting solenoids via high temperature superconductors," *IEEE Trans. Appl. Superc.*, vol. 18, no.2, pp. 70-81, June 2008 and included references.

[3] W. Schauer and W. Schelb, "Improvement of Nb3Sn high field critical current by a two-stage reaction," *IEEE Trans. Magnetics*, vol. 17, no. 1, pp. 374-377, Jan. 1981.

[4] R. Flukiger, W. Specking, M. Klemm, and S. Gauss, "Composite core Nb3Sn wires: preparation and characterization (invited)," *IEEE Trans. Magnetics*, vol. 25, no. 2, pp. 2192-2199, Mar. 1989.

[5] R. Zhou, **S.** Hong, and W. Marancik, "Artificial flux pinning in Nb and Nb3Sn superconductors," *IEEE Trans. Appl. Superc.*, vol. 3, no.1, pp. 986-989, Mar. 1993.

[6] S. Ochiai and K. Osamura, "Influence of grain size and upper critical magnetic field on global pinning force of bronze-processed Nb3Sn compound," *Acta Metall*, vol. 34, no. 12, pp. 2425-2433, Feb. 1986.

[7] D.R. Dietderich, M. Kelman, J.R. Litty, and R.M. Scanlan, "High critical current densities in Nb3Sn films with engineered microstructures – artificial pinning microstructures," *Advances in Cryogenic Engineering (Materials)*, vol. 44, 1998.

[8] D.R. Dietderich and R.M. Scanlan, "Nb3Sn artificial pinning microstructures," *IEEE Trans. Appl. Superc.*, vol. 7, no. 2, pp. 1201-1204, June 1997.

[9] C. Rodrigues and D. Rodrigues, Jr., "Flux pinning behavior of Nb3Sn superconductor with nanostructured pinning centers," *IEEE Trans. Appl. Superc.*, vol. 17, no. 2, pp. 2627-2630, June 2007.

[10] M.R. Shankar, S. Chandrasekar, W.D. Compton, and A.H. King, "Characteristics of aluminum 6061-T6 deformed to large plastic strains by machining," *Materials Science and Engineering A,* vol. 410-411, pp. 364-368, Mar. 2005.

[11] I. Chou, D.A. Koss, P.R. Howell, A.S. Ramani, "High temperature deformation of a mechanically alloyed niobium-yttria alloy," *Materials Science and Engineering A,* vol 222, pp. 14-20, Aug. 1997.

[12] R. Dolbec, M. Bolduc, X. Fan, J. Guo, J. Jurewicz, T. Labrot, S. Xue, and M. Boulos, "Nanopowder synthesis at industrial-scale production using the inductively-coupled plasma technology," *NSTI Nanotech 2008 Technical Proceedings,* vol 1, pp. 672-675, 2008.

[13] National High Magnetic Field Laboratory – Applied Superconductivity Center, "Engineering critical current density vs. applied field," *National High Magnetic Field Laboratory,* March 5, 2010. [Online]. Available: http://www.magnet.fsu.edu. [Accessed: March 21, 2010].

[14] M. R. Norman, “Modulated pairs in superconducting cuprates,” *Proceedings of the National Academy of Science,* vol. 105, pp.3173-3174, Mar. 2008.

[15] S. Horiuchi and E.Takayama-Muromachi, “Crystal Structure” in *Bismuth Based High-Temperature Superconductors*, Hiroshi Maeda and Kazumasa Togano, Eds. New York, NY: Marcel Dekker, 1996, pp. 7-32.

CONTACT INFORMATION

Name:	David Gabriel Rahmani
Professional Address:	c/o Dr. Peter McIntyre Department of Physics & Astronomy MS 4242 Texas A&M University College Station, TX 77843
Email Address:	david.rahmani@gmail.com
Education:	B.S., Physics, Texas A&M University, May 2010 Summa Cum Laude Undergraduate Research Scholar Texas A&M University Foundation Honors